U.S. ARMY COMBAT CAPABILITIES DEVELOPMENT COMMAND
CHEMICAL BIOLOGICAL CENTER

ABERDEEN PROVING GROUND, MD 21010-5424

CCDC CBC-TR-1623

Development of a Surface-Enhanced Raman Spectroscopy (SERS)-Based Microfluidic Device for Narcotics Detection

Neal D. Kline
Ashish Tripathi
Erik Emmons
Jason Guicheteau
Augustus W. Fountain III

RESEARCH AND TECHNOLOGY DIRECTORATE

March 2020

Disclaimer

The findings in this report are not to be construed as an official Department of the Army position unless so designated by other authorizing documents.

REPORT DOCUMENTATION PAGE

Form Approved
OMB No. 0704-0188

1. REPORT DATE *(DD-MM-YYYY)*	2. REPORT TYPE	3. DATES COVERED *(From - To)*
XX-03-2020	Final	Oct 2017–Sep 2019

4. TITLE AND SUBTITLE
Development of a Surface-Enhanced Raman Spectroscopy (SERS)-Based Microfluidic Device for Narcotics Detection

5a. CONTRACT NUMBER

5b. GRANT NUMBER

5c. PROGRAM ELEMENT NUMBER
622622 and 633004

6. AUTHOR(S)
Kline, Neal D.; Tripathi, Ashish; Emmons, Erik; Guicheteau, Jason; Fountain, Augustus W., III*

5d. PROJECT NUMBER
522 and L97

5e. TASK NUMBER
Task 08 and 03

5f. WORK UNIT NUMBER

7. PERFORMING ORGANIZATION NAME(S) AND ADDRESS(ES)
Director, CCDC CBC, ATTN: FCDD-CBR-IS, APG, MD 21010-5424

8. PERFORMING ORGANIZATION REPORT NUMBER
CCDC CBC-TR-1623

9. SPONSORING / MONITORING AGENCY NAME(S) AND ADDRESS(ES)

10. SPONSOR/MONITOR'S ACRONYM(S)

11. SPONSOR/MONITOR'S REPORT NUMBER(S)

12. DISTRIBUTION / AVAILABILITY STATEMENT
Approved for public release: distribution unlimited.

13. SUPPLEMENTARY NOTES
*Retired.
U.S. Army Combat Capabilities Development Command Chemical Biological Center (CCDC CBC) was previously known as U.S. Army Edgewood Chemical Biological Center (ECBC).

14. ABSTRACT: (Limit 200 words)
A microfluidic device is being developed by University of California, Santa Barbara as part of a joint effort with the U.S. Army to provide a portable, rapid drug-detection device for drugs and explosives. Surface-enhanced Raman spectroscopy (SERS) was used to provide a sensitive, selective detection technique within the microfluidic platform that employs metallic nanoparticles as the SERS medium. Issues with the device's performance, including reproducibility of flows and targeted binding of analytes, were identified as limitations of the technology. This report details the attempts to remedy these issues and make the technology field-deployable.

15. SUBJECT TERMS
Surface-enhanced Raman spectroscopy (SERS); Raman spectroscopy; Microfluidics; Narcotics detection; Nanoparticles; Klarite

16. SECURITY CLASSIFICATION OF:			17. LIMITATION OF ABSTRACT	18. NUMBER OF PAGES	19a. NAME OF RESPONSIBLE PERSON
a. REPORT	b. ABSTRACT	c. THIS PAGE			Renu B. Rastogi
U	U	U	UU	40	19b. TELEPHONE NUMBER *(include area code)* (410) 436-7545

Blank

PREFACE

The work described in this report was authorized under project nos. 522 and L97. The work was started in October 2017 and completed in September 2019. At the time this work was performed, the U.S. Army Combat Capabilities Development Command Chemical Biological Center (CCDC CBC; Aberdeen Proving Ground, MD) was known as the U.S. Army Edgewood Chemical Biological Center (ECBC).

The use of either trade or manufacturers' names in this report does not constitute an official endorsement of any commercial products. This report may not be cited for purposes of advertisement.

This report has been approved for public release.

Blank

CONTENTS

FIGURES

TABLE

Blank

DEVELOPMENT OF A SURFACE-ENHANCED RAMAN SPECTROSCOPY (SERS)-BASED MICROFLUIDIC DEVICE FOR NARCOTICS DETECTION

1. INTRODUCTION

Worldwide drug trade and drug use has increased significantly over the past several years, which poses a growing threat to the United States in terms of public health, national security, and the fight against terrorism.[1–5] The detection of illicit drugs or their metabolites in bodily fluids has proven to be an effective way to identify individuals who have used or come into contact with these drugs.[6] Some of the current analytical methods available for drug testing include gas chromatography with mass spectrometry, high-performance liquid chromatography, and enzyme-linked immunosorbent assay.[7–12] These analytical techniques are mostly performed in a laboratory environment by highly trained personnel. These tests require time-consuming, expensive pretreatment steps and reagents. Portable drug tests are available that rely on the Marquis reagent test or other colorimetric tests to determine the presence of illicit drugs.[13] However, such tests require specialized reactants and large sample volumes and can only screen for a limited number of possible drugs. Consequently, there exists a demand for drug-testing techniques that are portable, cheap, and selective and can be used to test for numerous substances.

Surface-enhanced Raman spectroscopy (SERS), combined with microfluidics, is a potential solution for a portable drug-testing platform. SERS is a form of vibrational spectroscopy that has become a valuable technique in nondestructive chemical analysis due to its high sensitivity and ability to discriminate between molecular species based on highly specific vibrational spectroscopic signatures. The foundation of SERS relies on the enhancement of normal Raman signatures of molecules that are adsorbed to an appropriately designed nanostructured substrate that is excited at its plasmon resonance.[14,15] Normal Raman signatures were enhanced up to 6–10 orders of magnitude, which makes the detection of single molecules possible using SERS.[16,17] Despite the tremendous advantages of SERS, its uses outside of the laboratory are impractical due to bulky and expensive laboratory equipment, lack of data reproducibility, and expensive substrates that are generally needed for high-sensitivity SERS detection. Combining SERS with a microfluidic platform provides a way to overcome these barriers.

Microfluidics is the science of manipulating and analyzing fluid flow in structures of submillimeter dimensions.[18–20] Microfluidic chip designs have the advantages of low fluid volumes and production on a mass scale that enables them to be disposable, cost-effective, and portable. Using microfluidics to design SERS platforms also allows for the careful control of the flow and interaction between liquids on a microscale and leads to more reproducible results. The selection of a SERS medium containing patterned, immobilized noble metal substrates or colloids, which are typically very cheap to synthesize, can produce large enhancement factors. Meinhart, Moskovits, and coworkers developed several variations of microfluidic/SERS platforms that demonstrate the detection of cancer cells and methamphetamine in bodily fluids and the detection of airborne molecules using colloidal nanoparticles as the sensing medium.[21–25] Multiple groups have also designed devices that use immobilized SERS substrates such as TiO_2

nanotubes, noble metal films over nanostructured black silicon, and noble metal electrodes to detect analytes including explosives and neurotransmitters.[26–29] Combining SERS with microfluidics has the potential to fill the current technological gap in portable, low-cost detection devices.

To incorporate SERS into a microfluidic device for drug detection, optimization of the SERS conditions is crucial. If colloidal nanoparticles are used as the SERS medium, the combination of nanoparticle material, nanoparticle size, excitation wavelength, and capping agent on the nanoparticle that allows the lowest detection limits need to be determined to achieve the best possible results within the microfluidic platform. Kline et al. optimized the SERS conditions for a series of analytes (i.e., methamphetamine, morphine, and cocaine), which produced the results presented in Table 1.[30]

Table 1. Limits of Detection (LODs) for Different Excitation Wavelengths, Nanoparticle Materials, and Capping Agents for the Different Analytes

Excitation Wavelength (nm)	**Nanoparticle Material**	**Capping Agent**	**Morphine LOD (M)**	**Cocaine LOD (M)**	**Methamphetamine LOD (M)**
532	Silver	Citrate	$8 \times 10^{-6} \pm 4 \times 10^{-6}$	$3 \times 10^{-5} \pm 4 \times 10^{-6}$	$9 \times 10^{-5} \pm 3 \times 10^{-5}$
		Tannate	$2.3 \times 10^{-6} \pm 3 \times 10^{-7}$	$1.2 \times 10^{-5} \pm 7 \times 10^{-7}$	$1.8 \times 10^{-5} \pm 1 \times 10^{-6}$
		Borate	$3.2 \times 10^{-6} \pm 5 \times 10^{-7}$	$3 \times 10^{-5} \pm 4 \times 10^{-6}$	$3 \times 10^{-4} \pm 1 \times 10^{-4}$
633	Silver	Citrate	$2.9 \times 10^{-6} \pm 3 \times 10^{-7}$	$1.8 \times 10^{-5} \pm 2 \times 10^{-6}$	$3 \times 10^{-5} \pm 5 \times 10^{-6}$
		Tannate	$5.0 \times 10^{-6} \pm 1 \times 10^{-6}$	$1.9 \times 10^{-5} \pm 2 \times 10^{-6}$	$4 \times 10^{-5} \pm 6 \times 10^{-6}$
		Borate	$1.4 \times 10^{-6} \pm 1 \times 10^{-7}$	$3.0 \times 10^{-5} \pm 4 \times 10^{-6}$	$3 \times 10^{-4} \pm 7 \times 10^{-5}$
	Gold	Citrate	$4.8 \times 10^{-8} \pm 1 \times 10^{-8}$	$9 \times 10^{-7} \pm 3 \times 10^{-7}$	$1 \times 10^{-6} \pm 1 \times 10^{-7}$
		Tannate	$2.1 \times 10^{-5} \pm 3 \times 10^{-6}$	$1.0 \times 10^{-4} \pm 7 \times 10^{-6}$	$5 \times 10^{-4} \pm 3 \times 10^{-4}$
		Borate	$4.7 \times 10^{-8} \pm 9 \times 10^{-9}$	$1.5 \times 10^{-8} \pm 1 \times 10^{-9}$	$3.0 \times 10^{-8} \pm 4 \times 10^{-9}$

The borate-capped, gold nanoparticles excited with a 633 nm laser gave the best results with LODs of 1.5×10^{-8} to 4.7×10^{-8} M (4.5–13 ng/mL), which are well within the ranges of physiologically relevant concentrations to determine drug use or exposure. Based on our results, Metrohm Raman (Laramie, WY) built a custom Raman spectrometer (Sierra 2.0) that operated at 633 nm for use in our experiments (Figure 1).

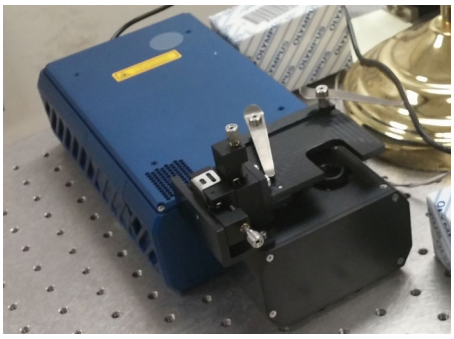

Figure 1. Custom Raman spectrometer from Metrohm Raman.

1.1 Characterization of Drugs in Artificial Bodily Fluids

After the optimal spectroscopic conditions for the design of the microfluidic/SERS detection platform were identified, the spectroscopic conditions were investigated in bodily fluid matrices. Experiments were conducted in artificial saliva and artificial urine that were purchased from Pickering Laboratories, Inc. (Mountain View, CA) and were conducted in the same manner as described by Kline, et al.[30] except that stock drug solutions and serial dilutions were prepared in artificial bodily fluids. Raman spectra were collected with the Sierra 2.0 system operating at 633 nm using 15 mW power on the samples. Data were also collected for the gold, borate-capped nanoparticles along with the silver, citrate-capped nanoparticles with the Sierra system.

SERS spectra collected for test analytes with the gold, borate-capped nanoparticles in artificial saliva and urine are presented in Figures 2 and 3, respectively. In Figures 2 and 3, the top panels are the data for cocaine, the middle panels are the data for morphine, and the bottom panels are the data for methamphetamine. In Figures 2 and 3, data on the left sides are the raw Raman spectra, whereas the data on the right sides were processed by the removal of the background trace through a partial least squares (PLS) subtraction. Several background features are present from the artificial bodily fluids that complicate the spectral analyses because some of them overlap with analyte spectral features. Artificial saliva has features at 450, 700, 850, and 890 cm^{-1}, whereas artificial urine has a singular feature around 1000 cm^{-1}.

Spectral features from the analyte are marked by an asterisk in Figures 2 and 3 to facilitate their identification from background signals. Cocaine and methamphetamine both have a band at 1000 cm^{-1} that is clearly visible in Figure 2 in the raw and PLS-processed data. In addition, methamphetamine has another band near 1200 cm^{-1}, and morphine has another band near 600 cm^{-1}. Identification of analyte bands was much more difficult with the artificial urine (Figure 3) because the bodily fluid matrix had a spectral feature near 1000 cm^{-1} where bands from cocaine and methamphetamine would be expected. No spectral features were marked in either the methamphetamine or cocaine because they were not able to be separated out definitively from the background. The morphine band at 600 cm^{-1} was sufficiently removed from any background in Figure 3 so that it could be clearly identified, and it was marked with an asterisk.

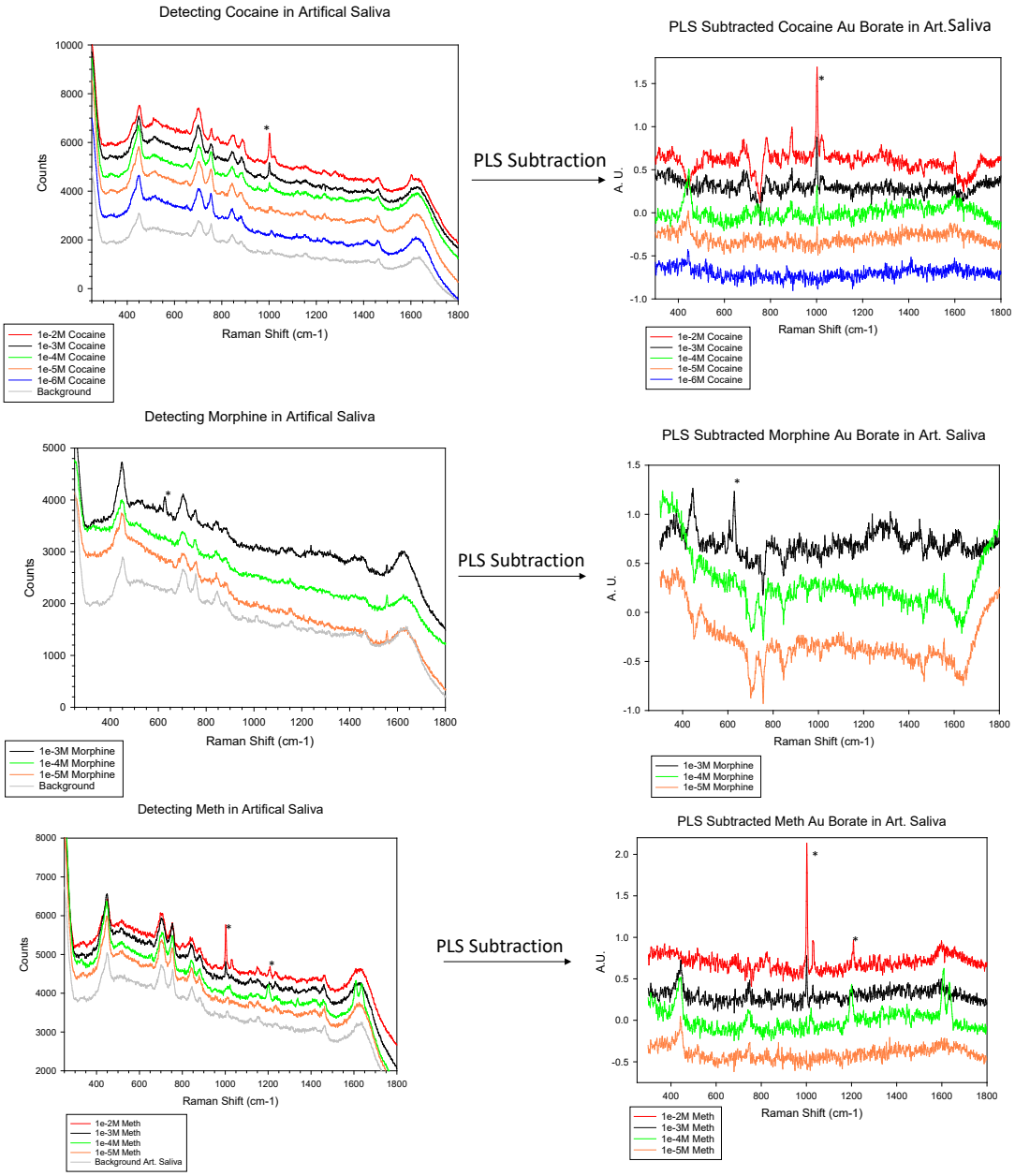

Figure 2. Experiments with target molecules in artificial saliva using gold, borate-capped nanoparticles.

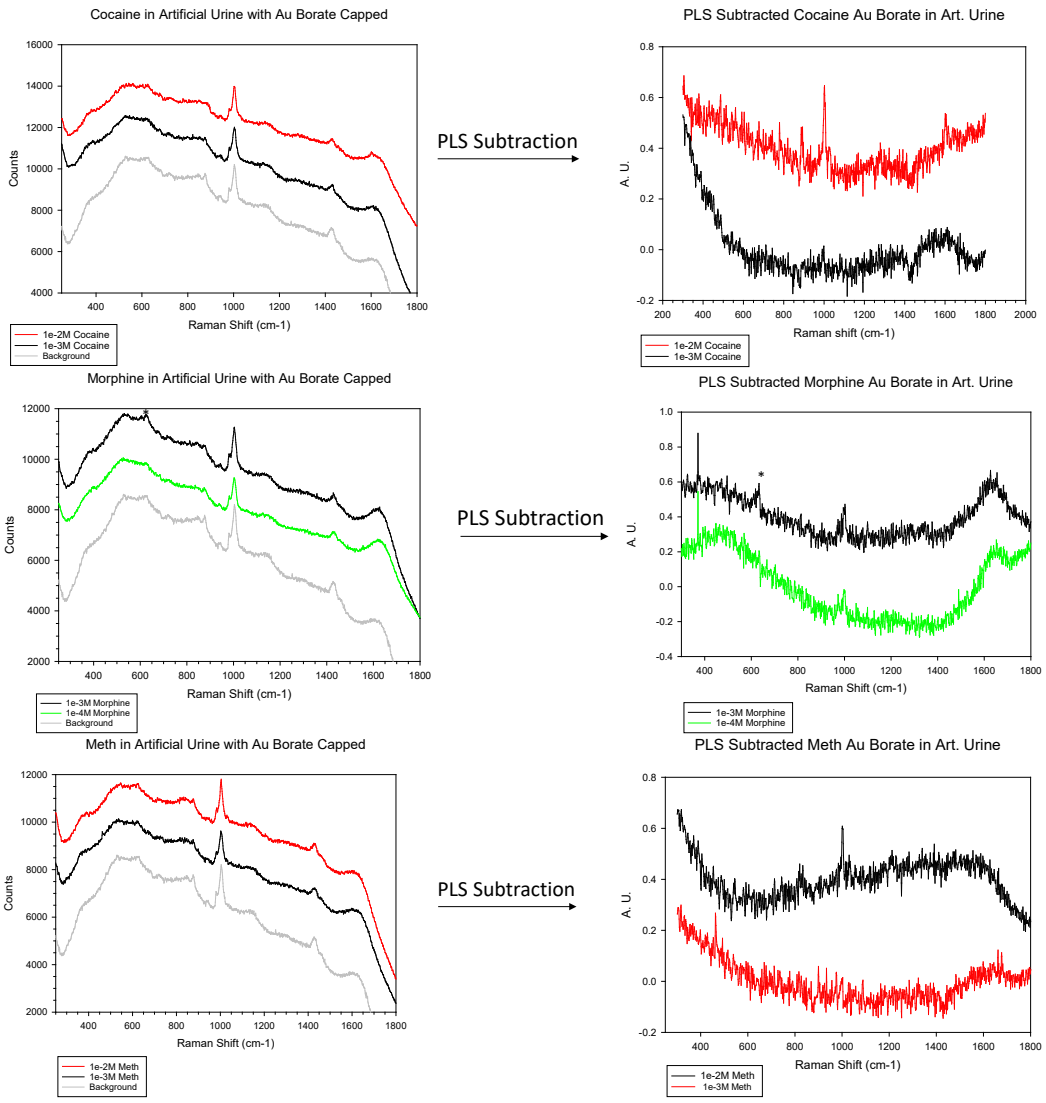

Figure 3. Experiments with target molecules in artificial urine using gold, borate-capped nanoparticles.

SERS spectra collected for test analytes with the silver, citrate-capped nanoparticles in artificial saliva and urine are presented in Figures 4 and 5, respectively. In Figures 4 and 5, the top panels are the data for cocaine, the middle panels are the data for morphine, and the bottom panels are the data for methamphetamine. In Figures 4 and 5, the data on the left sides are the raw Raman spectra, whereas the data on the right sides were processed by the removal of the background trace through a PLS subtraction. Several background features are present from the artificial bodily fluids that complicate the spectral analyses because some of them overlap with analyte spectral features. Artificial saliva has features at 450, 500, 640, 775, 800, 850, 925, 960, 1250, and 1460 cm^{-1}, whereas artificial urine has a singular feature around 1000 cm^{-1}.

Spectral features from the analyte are marked by an asterisk in Figures 4 and 5 to facilitate their identification from background signals. In Figure 4, cocaine has spectral features

at 850, 1000, 1300, and 1750 cm^{-1}; methamphetamine has spectral features at 1000, 1200, and 1600 cm^{-1}; and morphine has features near 600, 1000, 1250, 1350, 1500, and 1600 cm^{-1} that are clearly visible in the raw and PLS-processed data. Analyte bands were more easily identifiable with the silver nanoparticles in artificial urine (Figure 5) than with the gold nanoparticles (Figure 3). In Figure 5, cocaine has identifiable features at 850, 1000, 1300, and 1750 cm^{-1}; methamphetamine has spectral features at 1000 and 1200 cm^{-1}; and morphine has spectral features at 600 cm^{-1}. Several more features were observed in the SERS spectra of the analytes with the silver nanoparticles as compared with the gold nanoparticles. This was most likely due to a combination of the silver nanoparticles, which provide a larger enhancement than the gold nanoparticles, and because the molecules bind differently to the silver and gold surfaces.

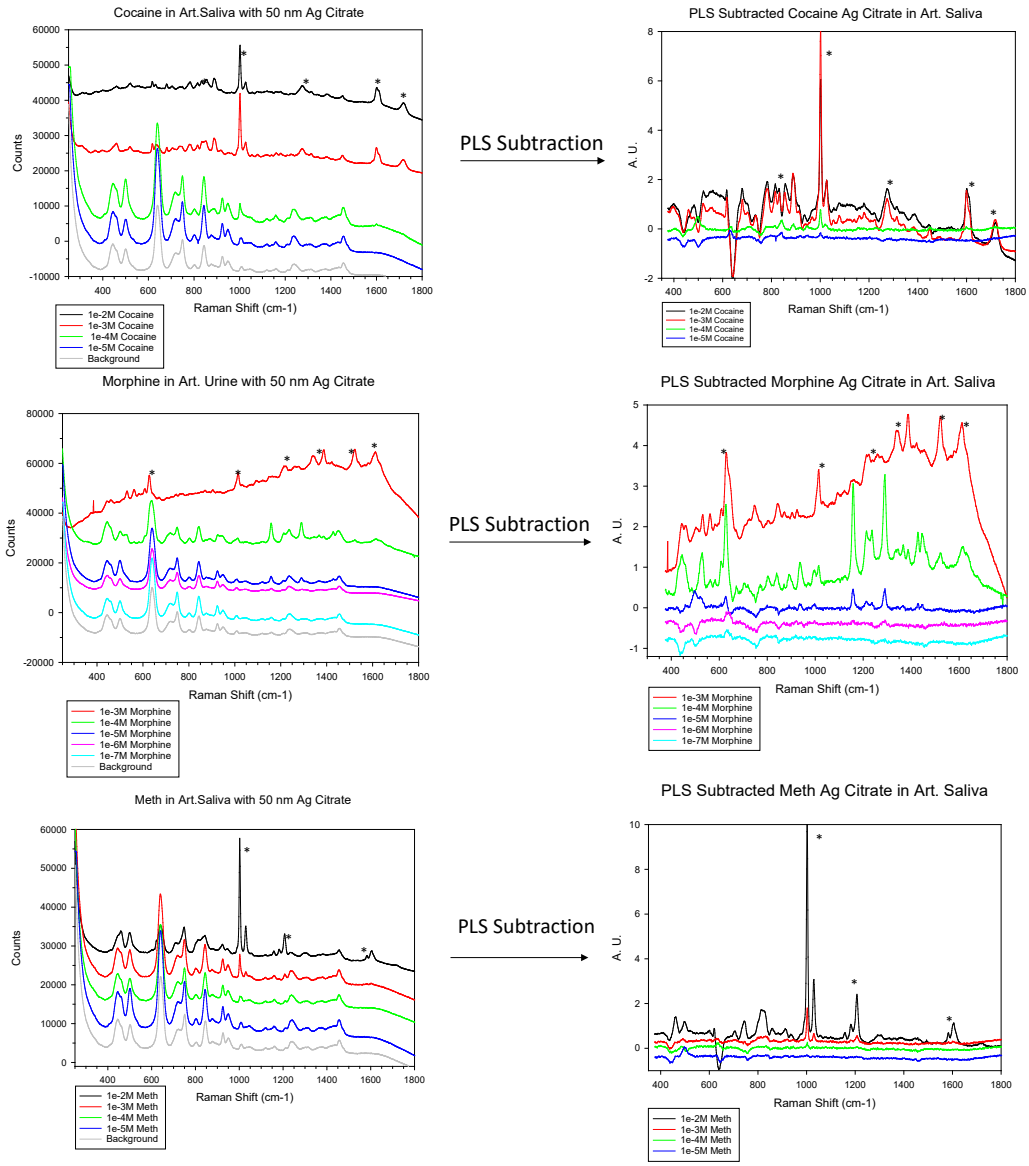

Figure 4. Experiments with target molecules in artificial saliva using silver, borate-capped nanoparticles.

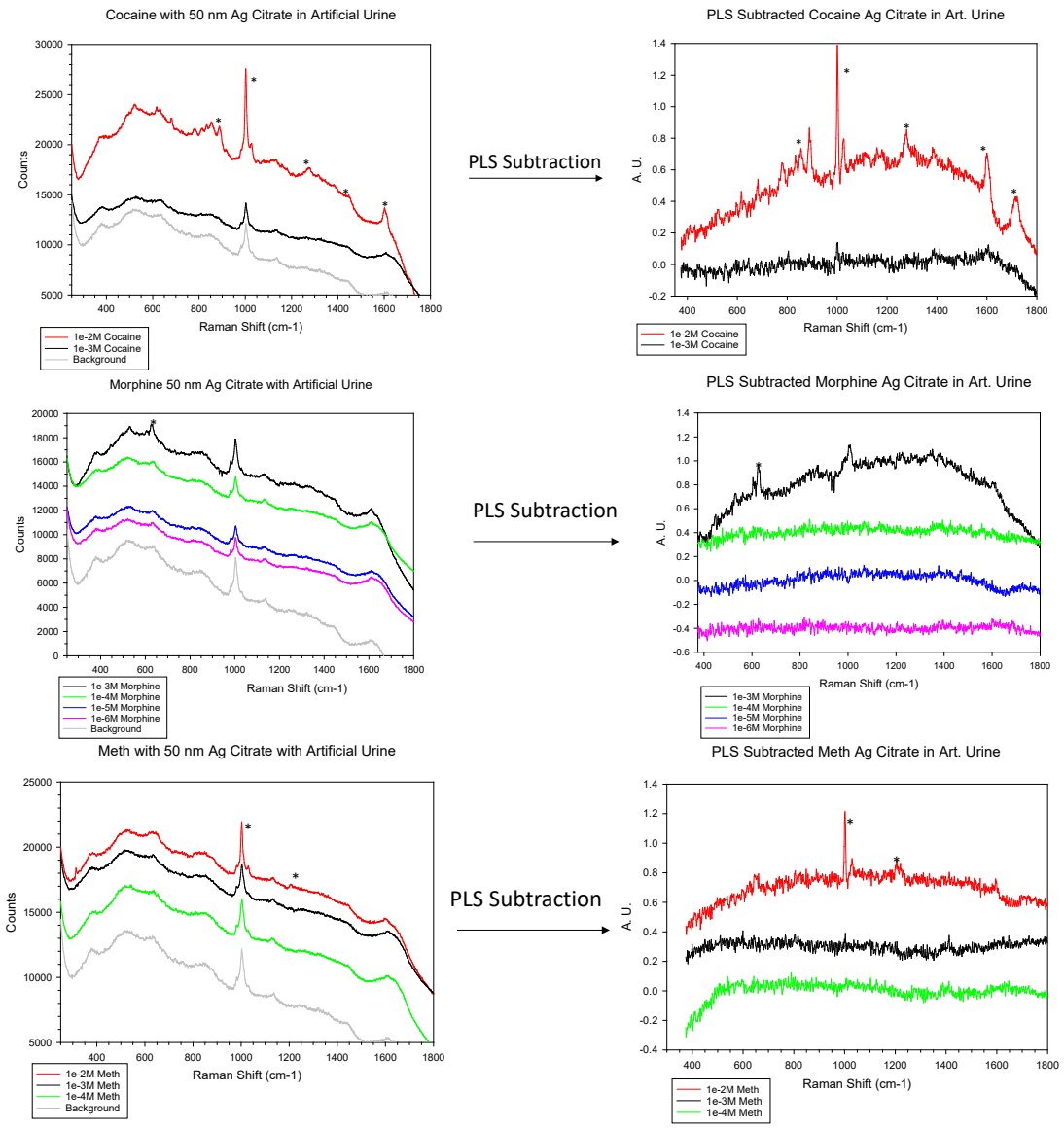

Figure 5. Experiments with target molecules in artificial urine using silver, borate-capped nanoparticles.

The LODs for the gold and silver nanoparticles in the artificial bodily fluids were worse than the LODs for the aqueous drug solutions. We obtained maximum LOD values of ~1×10^{-5} M for the gold nanoparticles and ~1×10^{-3} M for the silver nanoparticles, which were 3 orders of magnitude worse than the LODs obtained using the aqueous solutions. This could be due to larger background signals from the bodily fluids or the binding of bodily fluid to active sites on nanoparticles, which reduces sites available to target analytes and results in a worse LOD value.

1.2 Characterization of Drugs in Microfluidic Chips

After experimenting with the colloids in bodily fluid matrices, we also wanted to investigate how the detection scheme performed on a microfluidic chip. Figure 6 shows the Sierra 2.0 with the microfluidic chip attachment and demonstrates the on-chip analysis.

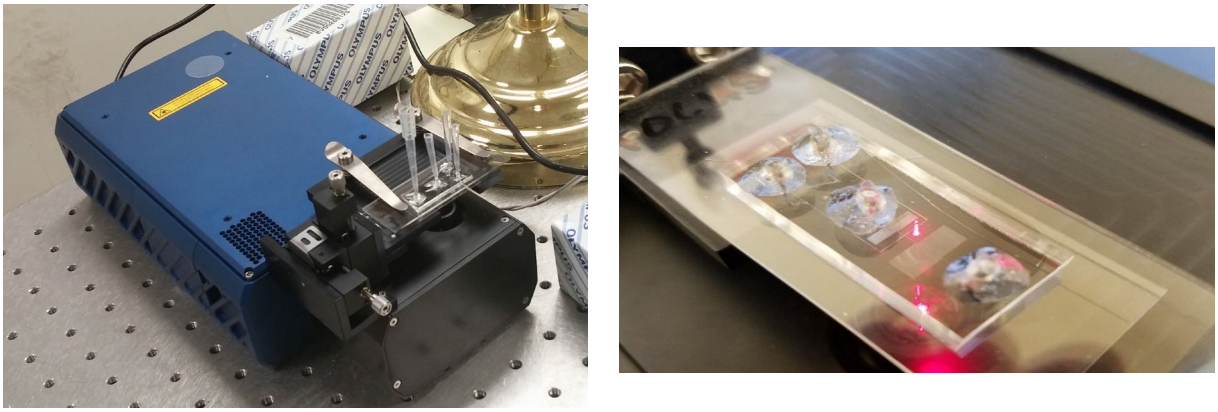

Figure 6. (Left) Sierra 2.0 system with microfluidic chip attachment for on-chip analysis. (Right) close-up view of the chip attachment.

The microfluidic chips were supplied by University of California, Santa Barbara (UCSB), and an illustration of how they work is shown in Figure 7. There are three inlet channels: colloid, analyte, and salt (for crashing colloid) with an outlet that has a vacuum attached to apply suction to the device and pull the liquids through the inlet tubes. The chip is designed to work around the concept of hydrodynamic focusing, which is achieved by introducing streams of different flow rates into a flow cell. The chip is also designed to create a laminar flow between the two streams. A laminar flow barrier is created between the streams that prevents the liquid in the streams from mixing. However, small particles in the streams can mix by diffusion across the laminar flow barriers that are created by the hydrodynamic focusing. In the UCSB microfluidic chips, the middle channel (analyte) is introduced at a flow rate one-quarter that of the two outside channels (colloid and salt). Hydrodynamic focusing is then achieved at the junction where all the streams meet. Although the streams are flowing after the junction, the small molecule drugs or drug metabolites will diffuse across the laminar flow barrier and attach to the surface of the nanoparticle. Likewise, the salt will diffuse across the channel and induce aggregation of the nanoparticles after the analytes have attached to the nanoparticle surface. The resulting crashed colloid can be probed by the SERS.

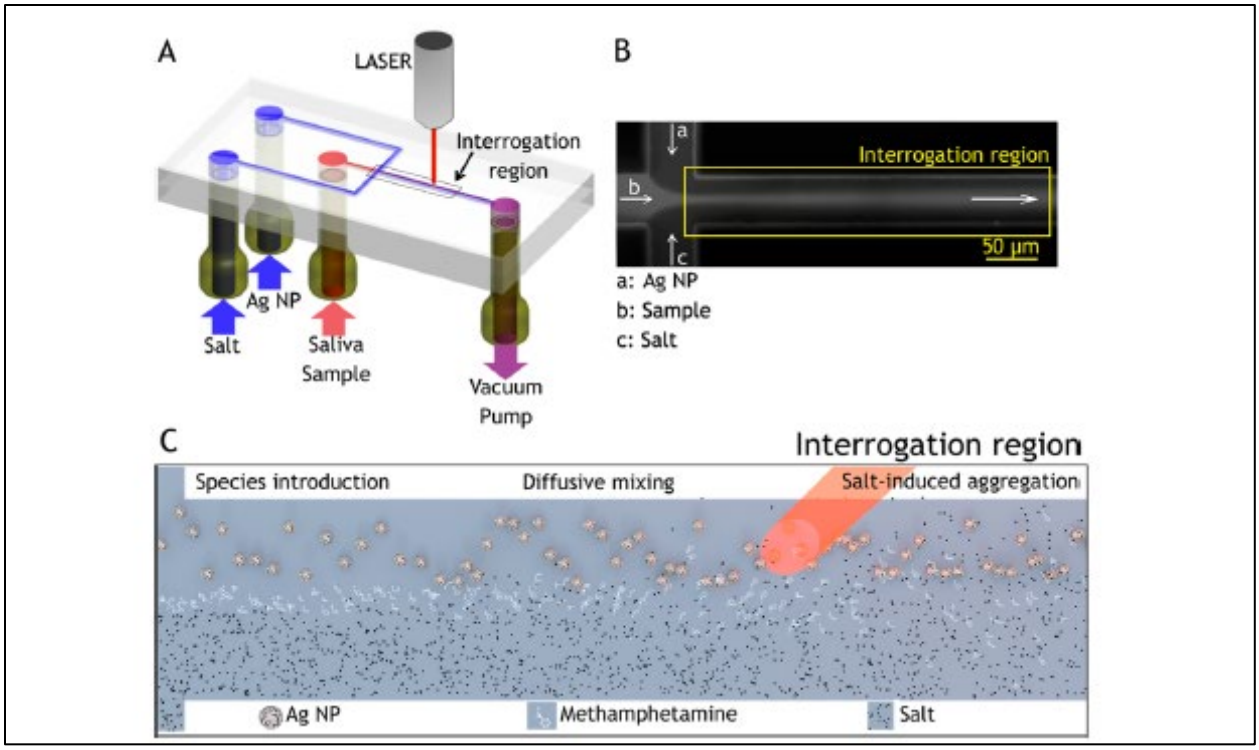

Figure 7. Diagram showing how microfluidic chips would achieve on-chip separation in a complex mixture.

SERS spectra collected for test analytes with the gold, borate-capped nanoparticles in the microfluidic chips are presented in Figure 8. In Figure 8, the top panel shows the data for methamphetamine, the middle panel shows the data for cocaine, and the bottom panel shows the data for morphine. In Figure 8, the data on the left side are the raw Raman spectra, whereas the data on the right side were processed by the removal of the background trace through a PLS subtraction. Several background features are present from the microfluidic chip that arises from the polydimethylsiloxane (PDMS) they were fabricated from. PDMS has features at 490, 625, and 710 cm^{-1}.

Spectral features from the analyte are marked by an asterisk in Figure 8 to facilitate their identification from background signals. In Figure 8, methamphetamine has spectral features at 1000 and 1250 cm^{-1}; cocaine has spectral features at 900 and 1000 cm^{-1}; and morphine has spectral features at 375, 625, 725, 790, 820, and 930 cm^{-1} that are clearly visible in Figure 4 in the raw data and PLS. The LODs obtained in the microfluidic chip were around the 1×10^{-6} M range, 2 orders of magnitude lower than those observed in the aluminum-coated glass cups and out of the range necessary for detecting drugs at physiological concentrations.

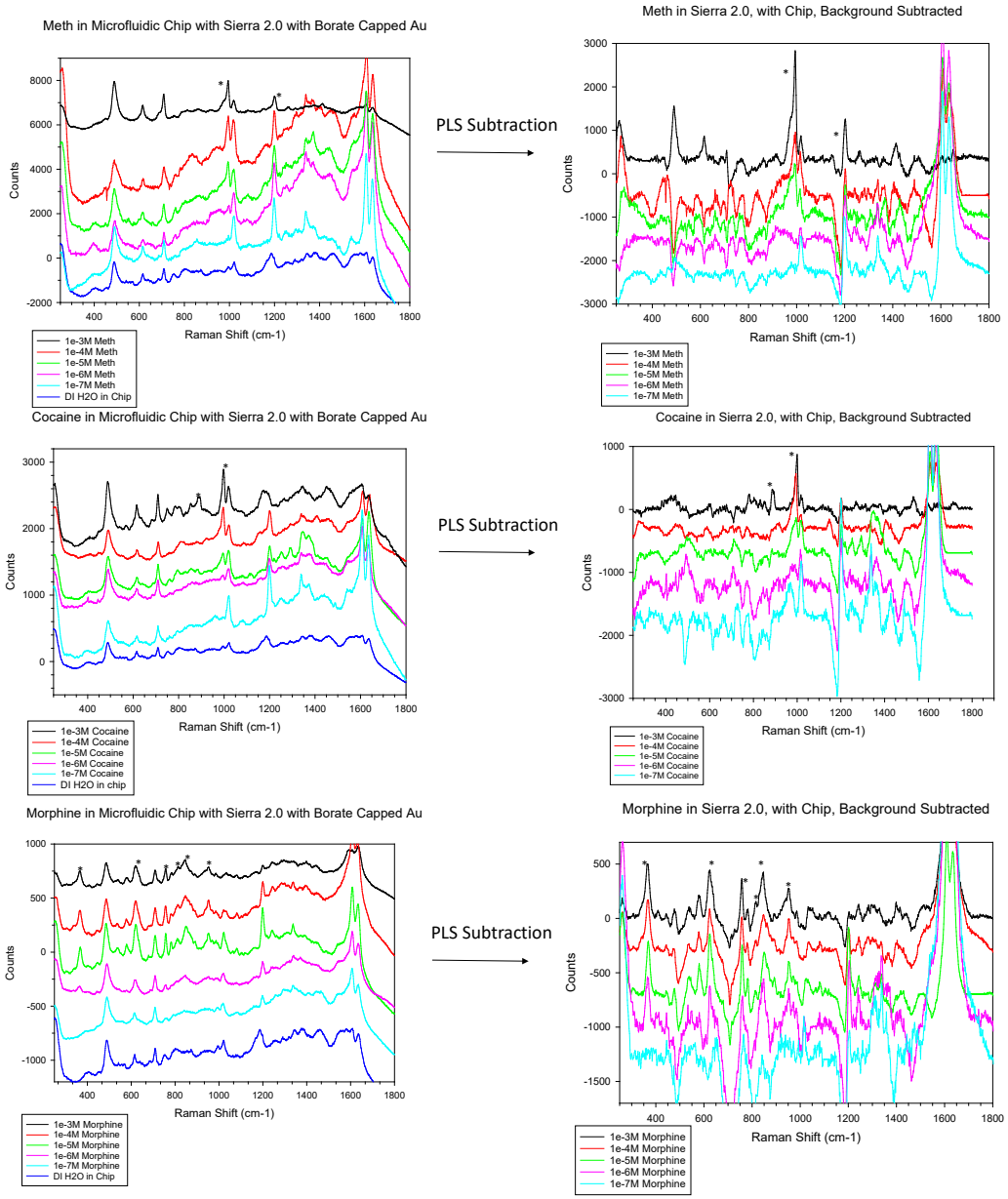

Figure 8. Determining LODs for target molecules in microfluidic device. Asterisks denote spectral features from target molecules.

Several issues were revealed upon moving from the aqueous solutions in the glass cups to bodily fluid matrices and the microfluidic platform to conduct experiments:

- Flows were inconsistent in the microfluidic chip.
- Bubble formations and clogging were constant problems in the chip.
- Background interferences made analyte detection more difficult in bodily fluids.
- LODs in the microfluidic chip were out of physiological range.

- Aligning the laser from the Metrohm Raman spectrometer properly in the colloidal-crashing region of the microfluidic chip was difficult and time-consuming.

Under a 6.2-funded initiative, members of the U.S. Army Combat Capabilities Development Command Chemical Biological Center (Aberdeen Proving Ground, MD) Spectroscopy Branch were able to investigate several of the aforementioned problems to make microfluidics a more attractive platform for sensing. A LabSmith, Inc. (Livermore, CA) microfluidic workstation, including syringe pumps for different microfluidic channels, three-way valves, and a breadboard system, was procured to aid in controlling flows within a microfluidic device. Paper-based microfluidics were also investigated for more controlled fluid flow in a device. Targeting of specific analytes was investigated by functionalizing gold nanoparticles and with single-strand deoxyribonucleic acid (ssDNA) aptamers and functionalizing Klarite planar substrates (Renishaw Diagnostics Ltd., Glasgow, U.K.) using thiolated compounds that were capable of binding our targets. By exploring these paths, we hope to achieve more consistent flows, reduce bubble formation in the microfluidic chip, and improve LODs by targeting specific analytes.

2. IMPROVING FLOW IN MICROFLUIDIC CHIPS

2.1 LabSmith Workstation

A key factor in the creation of high-performance microfluidic chips is the ability to manipulate their fluid flows. Our previous experiments (Section 1.2) were significantly hindered by the inability to create consistent flows within the device. One way to exert more control of fluid flows is through the use of syringe pumps to apply positive pressure to the inlets, in addition to performing suction on the waste channel. A LabSmith microfluidic workstation (Figure 9) was procured and characterized.

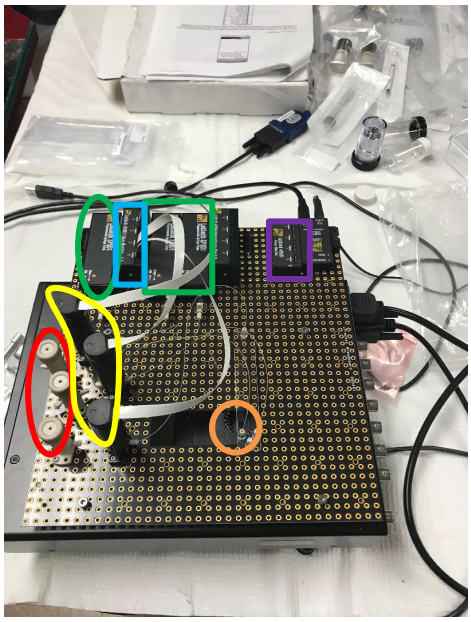

Figure 9. LabSmith microfluidic workstation. Reservoirs for holding liquids (red), three-way valves (yellow), syringe pumps (green), three-way valve controller (blue), power supply/computer interface in purple, and visualization objective (orange).

The workstation was equipped with a breadboard and several individual pieces that could be custom-arranged depending on the experiment to be run. The station also had its own software interface (uProcess; Figure 10) that could control the individual components on the breadboard, such as the syringe pumps and three-way valves. Liquids to be pumped through the microfluidic device were held in reservoirs that were attached to the breadboard and could be extracted from the reservoirs and into the microfluidic device by pulling the liquid through the three-way valves and into the syringe pumps. At that point, the channel of the valves would be changed, and the syringe pumps would push the liquids through the 1/16 in. polyetheretherketone tubing in the device. The system also came with a visualization tool that allowed real-time video and photographic capability so the user can monitor the flows on the microfluidic chip and pinpoint any problems. After setting up the microfluidic workstation, we began characterizing fluid flows to see how consistent they were through the devices. Representative examples of these observations are shown in Figures 11–14.

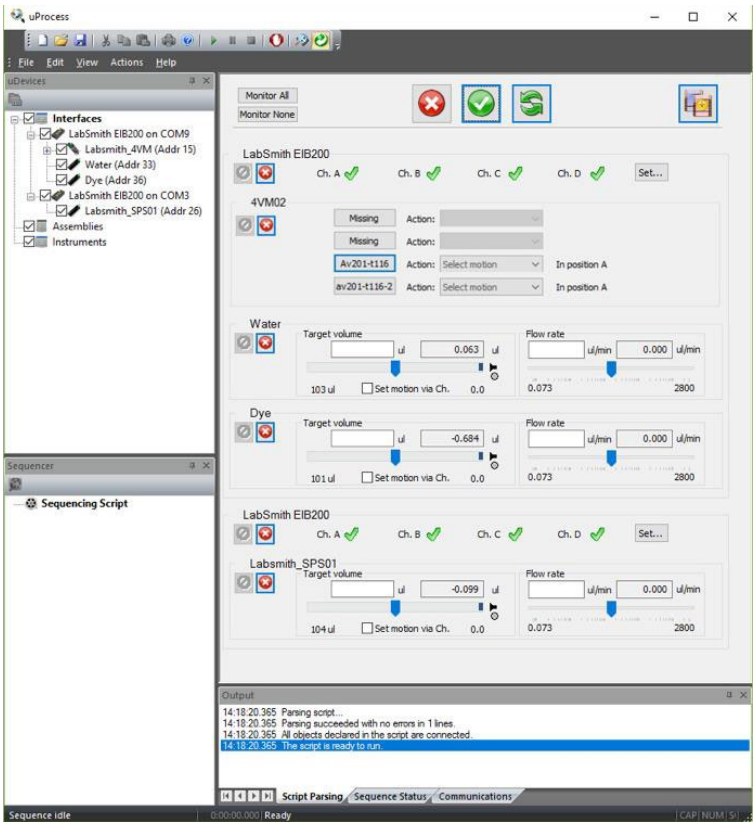

Figure 10. LabSmith uProcess software dashboard for controlling different microfluidic components.

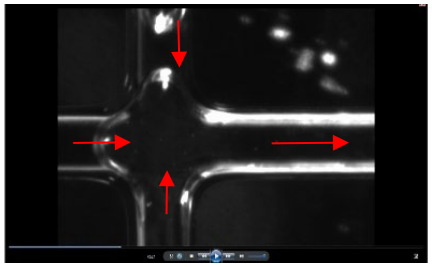

Figure 11. Screen capture of video showing flow in microfluidic device. Water is being driven by positive pressure from syringe pumps from top, bottom, and left channels. Waste is going to channel on right after four-way junction.

Figure 12. Screen capture of video showing flow in microfluidic device. Water is being driven by positive pressure from syringe pumps from top, bottom, and right channels. Waste is going to channel on left after four-way junction.

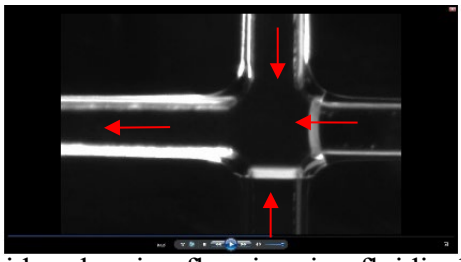

Figure 13. Screen capture of video showing flow in microfluidic device. Water is being driven by positive pressure from syringe pumps from top, bottom, and right channels. Bottom valve appears to be closed; therefore, waste is going to channel on left after four-way junction.

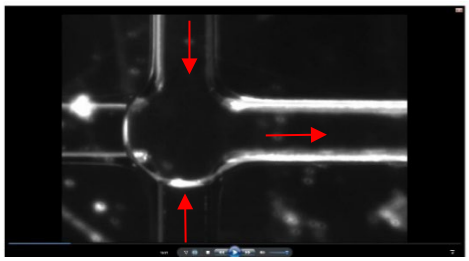

Figure 14. Screen capture of video showing flow in microfluidic device. Water is being driven by positive pressure from syringe pumps from top and bottom channels. Negative pressure is acting on the waste channel to the right, pulling the liquid.

Even with the implementation of the syringe pumps giving us more control over fluid flows, inconsistent flows and bubbling continued to be problems in the devices. The liquids being pumped through the channels would arrive at the junction at different times even though measures were taken to eliminate any "dead volume" present in the tubing and all syringe pump flow rates were the same. Different arrival times would cause liquid in one channel to back up the liquid in one or both of the other channels. Numerous techniques to introduce the fluid to the microfluidic chip were tried, such as: varying syringe pump flow rates, only introducing fluid through two channels instead of three, and using negative pressure on the waste channel to pull liquid through. None of the schemes that were tried yielded any better results toward achieving a more consistent fluid flow through the microfluidic device.

2.2 Paper-Based Microfluidics

We received a set of paper-based microfluidic devices (PBMFDs) that were manufactured by the Martinez Group of California Polytechnic State University (San Luis Obispo, CA). The devices were made with procedure outlined in the earlier reported work by Gaillard et al.[9] The PBMFDs were prepared using wax-based printing to create hydrophobic barrier boundaries along a 300 µm wide microfluidic channel of about 1 cm in length. Preliminary experiments with this single-channel PBMFD were conducted using the same gold–colloid with 60 nm particles and borate-capping, as described in Section 1.1. A 5×10^{-5} M concentration of methamphetamine was used as an analyte. Two 20 µL aliquots of gold–colloid were deposited in two different locations along the channel. Figure 15 shows the PBMFD and the location where the colloidal solution was deposited.

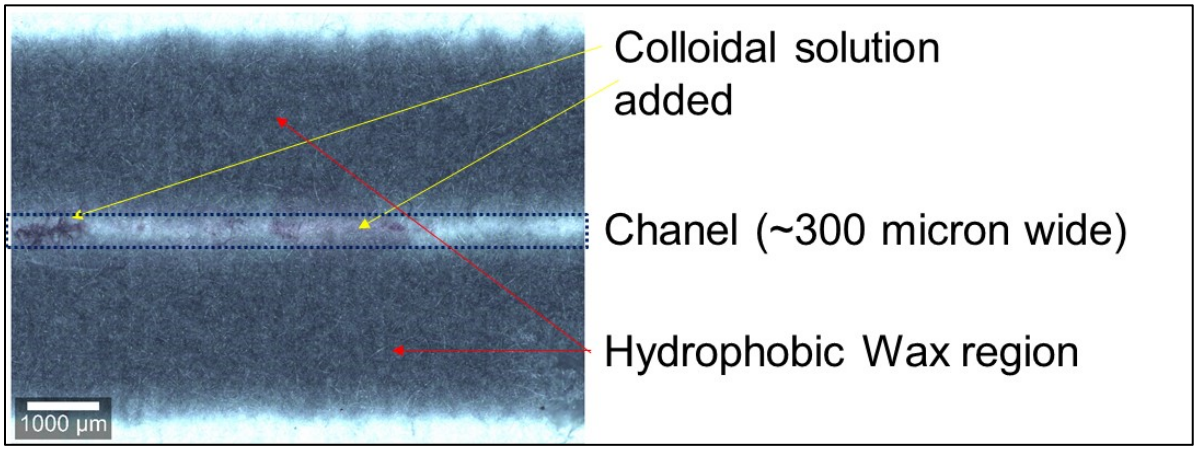

Figure 15. The layout of a PBMFD with colloidal residue locations.

After drying, a 20 µL aliquot of a solution containing 5×10^{-5} M methamphetamine and 1 M lithium chloride was added to one of the colloidal spots. The solution was allowed to dry. A multi-laser WITec 300-RA Alpha Raman microscope (WITec; Wissenschaftliche Instrumente und Technologie GmbH; Ulm, Germany) was used with the 633 nm laser set at 1 mW and with the 50× objective and True-Surface autofocus. Integration time was set to 2 s per spectrum, and the images were acquired with continuous travel mode. A 300 g/mm grating, centered at 750 nm, was used to obtain Raman spectra.

Various regions on the prepared PBMFD were interrogated with the Raman microscope. Figure 16 shows the locations of the regions that were analyzed with Raman microscope. The Raman analysis was performed on a blank fiber (background) with the colloidal residue in contact with the wax barrier and the colloidal residue in the microfluidic channel in contact with the analyte residue.

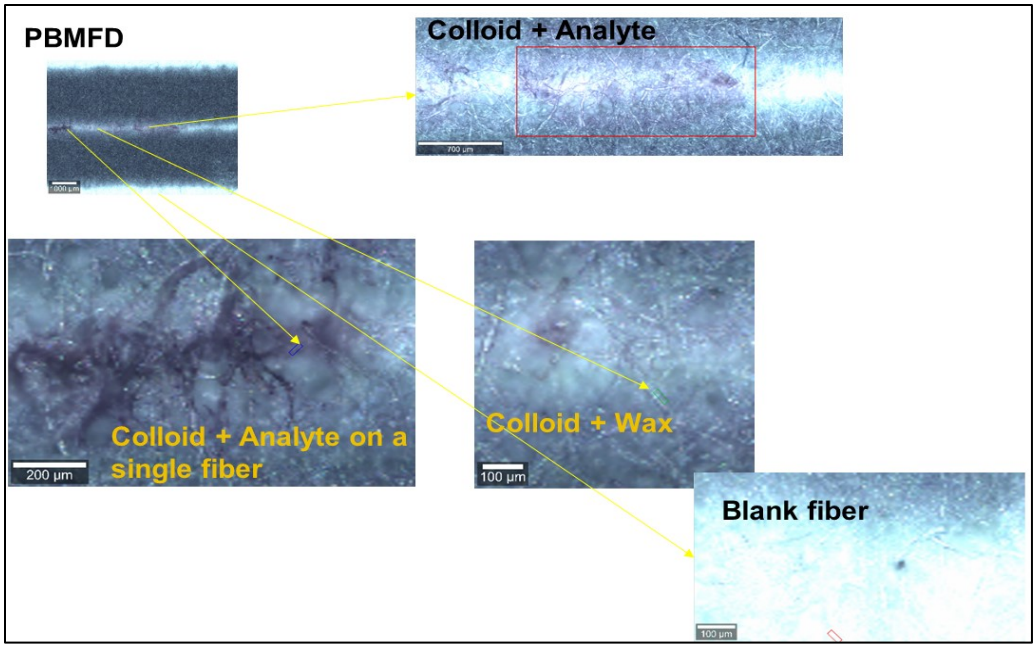

Figure 16. The locations of the regions on the PBMFD that were analyzed with Raman microscope.

2.2.1 Blank Fiber Region

A region of PBMFD outside the wax barrier was analyzed with the WITec Raman microscope. Because no SERS colloid was deposited in this region, there was no plasmonic enhancement obtained. Figure 17 shows the noisy average Raman spectra obtained from the untreated fiber; this noise was due to the low laser power (1 mW) and integration time (2 s) used to obtain the Raman spectra.

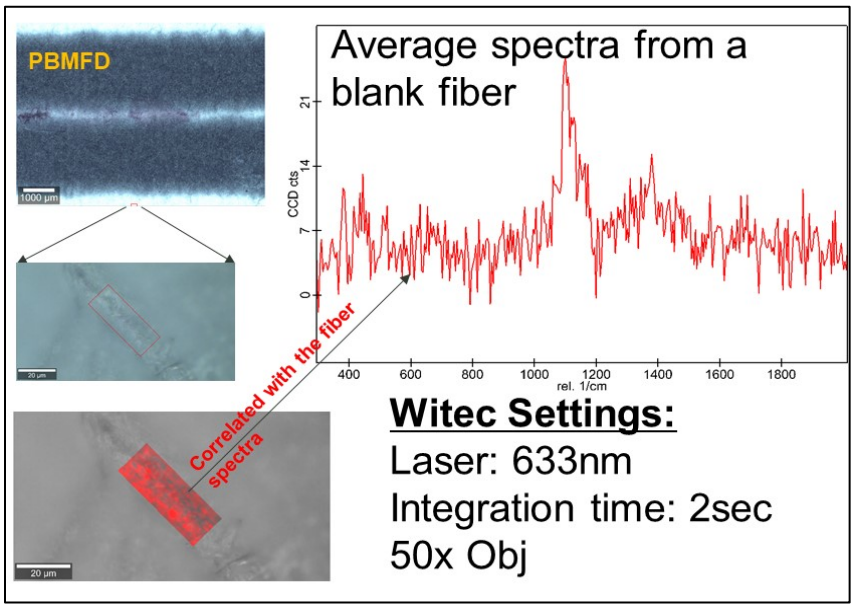

Figure 17. Blank fiber analysis with Raman chemical imaging (RCI) microscope.

2.2.2 Methamphetamine in SERS Colloid-Laced Microfluidic Channel

A region along the microfluidic channel was laced with 20 µL of gold–colloid with 60 nm particles and borate-capping. After the SERS colloidal solution was allowed to dry, a 20 µL aliquot of 5×10^{-5} M methamphetamine and a 20 µL aliquot of 1 M lithium chloride were added to the colloidal residue spot. The solution was allowed to dry. The resultant area of interest in the microfluidic channel was interrogated with the WITec Raman microscope. Two types of Raman analyses were performed: a scan of a large area of interest and a single fiber scan. Figure 18 shows the results of the large area scan. There seems to be the presence of the major vibrational modes from methamphetamine–SERS spectra, as was reported in Section 1.1 of this report. A single fiber in the microfluidic channel, which was laced with both the SERS colloid and methamphetamine, was also analyzed with the WITec Raman microscope. Figure 19 shows the results from the single cellulosic fiber interrogation using the Raman microscope. Major vibrational modes from methamphetamine–SERS spectra also seem to be present, as reported herein. However, the uniform distribution of regions on the fiber that show the methamphetamine–SERS interaction was not observed.

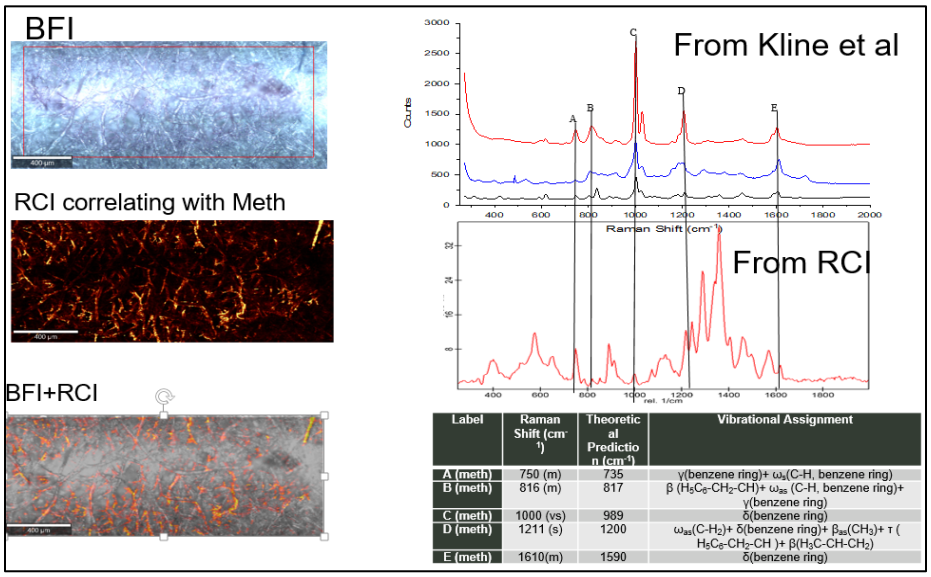

Label	Raman Shift (cm⁻¹)	Theoretical Prediction (cm⁻¹)	Vibrational Assignment
A (meth)	750 (m)	735	γ(benzene ring)+ ω_s(C-H, benzene ring)
B (meth)	816 (m)	817	β (H_5C_6-CH_2-CH)+ ω_{as} (C-H, benzene ring)+ γ(benzene ring)
C (meth)	1000 (vs)	989	δ(benzene ring)
D (meth)	1211 (s)	1200	ω_{as}(C-H_2)+ δ(benzene ring)+ β_{as}(CH_3)+ τ (H_5C_6-CH_2-CH)+ β(H_2C-CH-CH_2)
E (meth)	1610(m)	1590	δ(benzene ring)

Figure 18. Results from the RCI of a large area of interest that was laced with both colloid and methamphatamine.

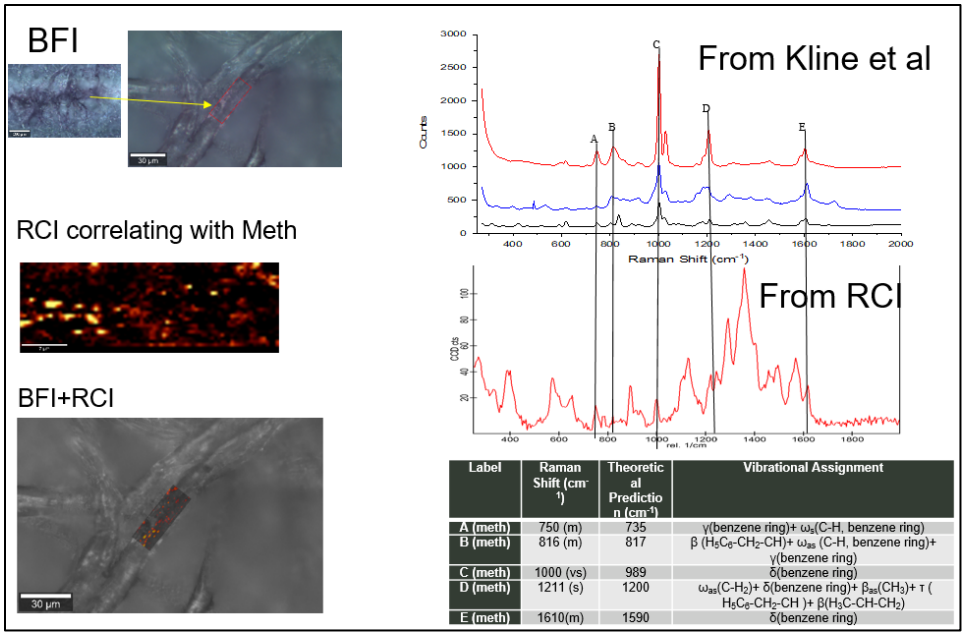

Figure 19. Results from the RCI of a single cellulosic fiber that was laced with both colloid and methamphetamine.

2.2.3 Wax–SERS Region

To ascertain that the marked spectral features observed in Figures 18 and 19 were due to the presence of methamphetamine and were not due to SERS spectral contribution from the wax and the dyes comprising the wax printer media, we used the WITec Raman microscope to interrogate a region where the SERS colloid made contact with the wax media. Figure 20 shows the results of this examination of the wax–SERS colloid region. The features at 750 and 1211 cm^{-1} were found in the wax–SERS spectra and in the methamphetamine–SERS spectra. Clearly, a cursory glance of the extracted wax spectrum finds agreement with similarly extracted spectra from methamphetamine–SERS region. Figure 21 shows a comparison of the methamphetamine–SERS spectra that were obtained via a large area scan (Figure 18) and a single cellulosic fiber scan (Figure 19) with those spectra obtained from the wax–SERS region (Figure 20). The left panel of Figure 21 shows the comparison of these spectra with those reported from the methamphetamine–SERS analysis discussed herein. The right panel shows the same comparison after subtracting the spectral contributions from wax–SERS region. Clearly, the features at the 1000 and 1600 cm^{-1} spectral regions match, but many others are missing. This experiment points to the complexity of SERS analysis with a paper-based microfluidic device and warrants further investigation.

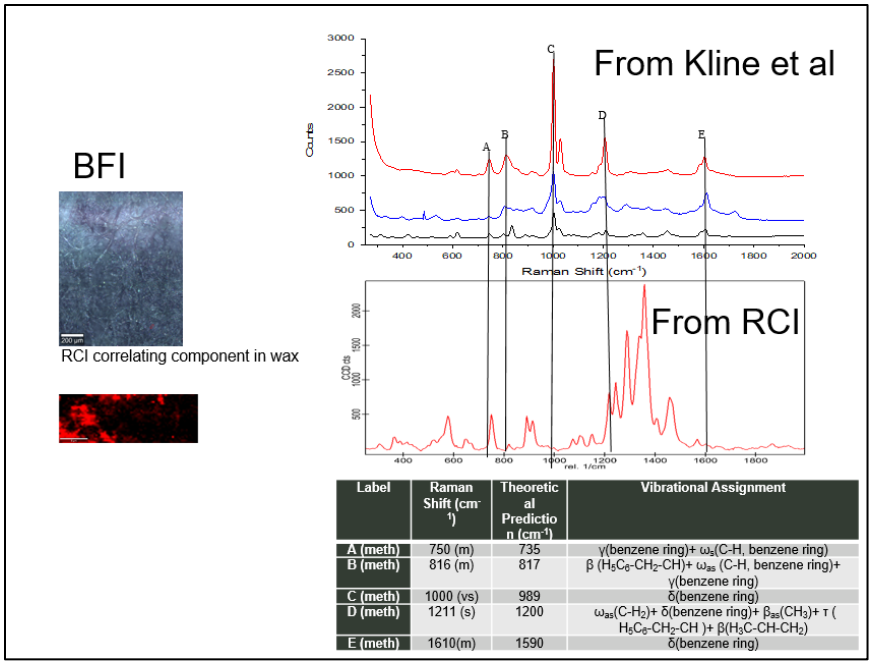

Label	Raman Shift (cm-1)	Theoretical Prediction (cm-1)	Vibrational Assignment
A (meth)	750 (m)	735	γ(benzene ring)+ ω_s(C-H, benzene ring)
B (meth)	816 (m)	817	β (H_5C_6-CH_2-CH)+ ω_{as} (C-H, benzene ring)+ γ(benzene ring)
C (meth)	1000 (vs)	989	δ(benzene ring)
D (meth)	1211 (s)	1200	ω_{as}(C-H_2)+ δ(benzene ring)+ β_{as}(CH_3)+ τ (H_5C_6-CH_2-CH)+ β(H_3C-CH-CH_2)
E (meth)	1610(m)	1590	δ(benzene ring)

Figure 20. Raman imaging analysis of wax–SERS–colloidal region.

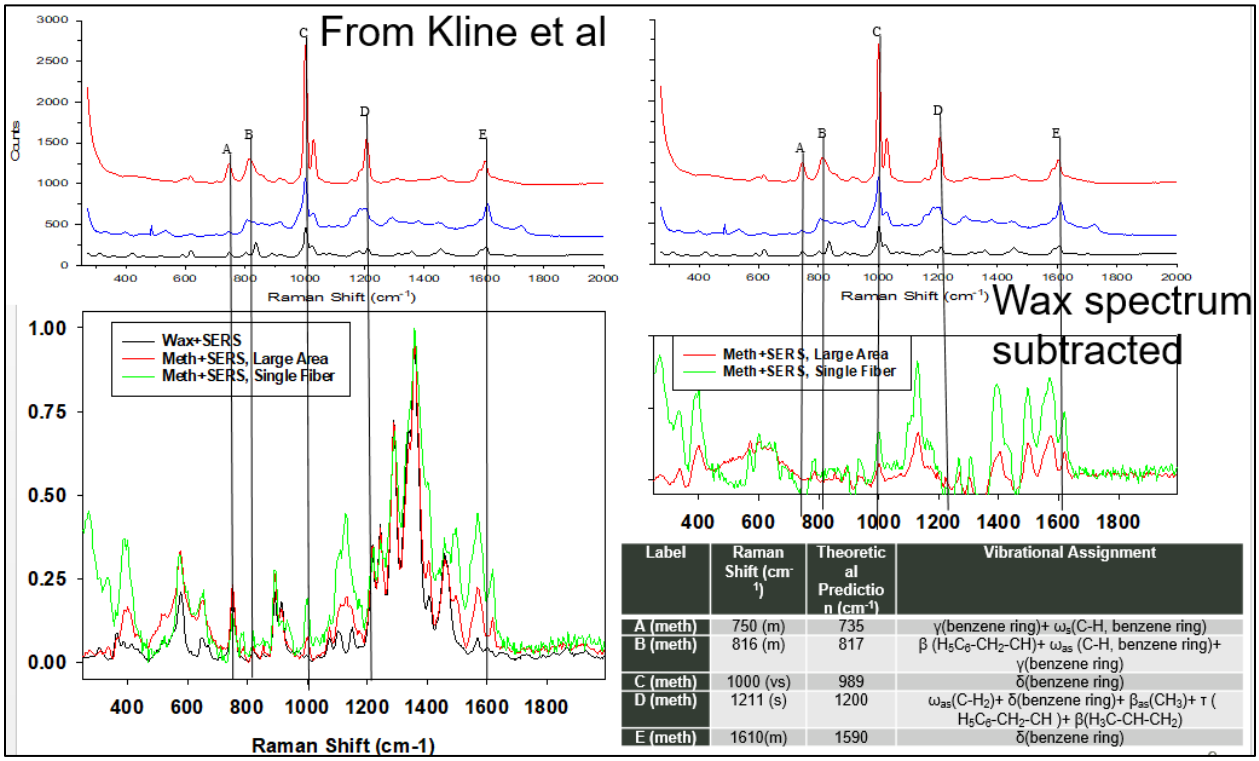

Label	Raman Shift (cm-1)	Theoretical Prediction (cm-1)	Vibrational Assignment
A (meth)	750 (m)	735	γ(benzene ring)+ ω_s(C-H, benzene ring)
B (meth)	816 (m)	817	β (H_5C_6-CH_2-CH)+ ω_{as} (C-H, benzene ring)+ γ(benzene ring)
C (meth)	1000 (vs)	989	δ(benzene ring)
D (meth)	1211 (s)	1200	ω_{as}(C-H_2)+ δ(benzene ring)+ β_{as}(CH_3)+ τ (H_5C_6-CH_2-CH)+ β(H_3C-CH-CH_2)
E (meth)	1610(m)	1590	δ(benzene ring)

Figure 21. Spectral comparison of methamphetamine–SERS spectra obtained via large area and single cellulosic fiber scans with the wax–SERS spectra.

3. TARGETED BINDING OF ANALYTES

3.1 Functionalizing Klarite Substrates

The SERS technique has potential for use in the trace detection of compounds of interest (COIs). However, the effectiveness of SERS to detect COIs such as narcotics and energetics is largely dependent on the binding affinity of these COIs to the metallic component of the SERS substrate. Our previous work has demonstrated[31,32] that binding affinity has a measureable influence on the SERS enhancement value. We used gold-coated Klarite substrate for the planar-array SERS experiments. Although this substrate provides reproducible results, gold does not exhibit high binding affinity toward many of the functional groups that are present in COIs. To overcome this challenge, we explored functionalizing the gold substrate with a molecule that binds readily to gold and is stable over the experimentation time. An example of this type of functionalization was reported by Chen et al.[33] Chen and his coworkers reported detection of trinitrotoluene (TNT) with gold nanoparticles functionalized with 4-aminothiophenol (4-ATP). The researchers claim an LOD of 10^{-11} M concentration of TNT in water with this system.

Following the approach outlined by Chen et al., we functionalized Klarite substrate with 4-ATP by submerging gold–Klarite chips in 10^{-4} M aqueous solution of 4-ATP for 30 min. These 4-ATP functionalized Klarite chips were examined with a Jasco NRS-3200 Raman microscope system (Jasco Analytical Instruments; Easton, MD) to confirm the binding of 4-ATP. An excitation wavelength of 785 nm was used, which yielded good SERS enhancement with the gold-coated Klarite substrates. A 10× microscope objective and a laser power of ~4–5 mW were used in this analysis. This relatively low magnification and low laser power were previously shown to minimize thermal or photodegradation effects. A 600 g/mm grating was used to disperse the Raman scattered light, which was detected with a thermoelectrically cooled charge-coupled device camera (Andor Technology, Oxford Instruments; Belfast, Ireland). The Rayleigh scattered light was suppressed with a rejection filter (Semrock, IDEX Health and Science; Rochester, NY). We explored the possible trace detection of three narcotics (morphine, methamphetamine, and cocaine) and three energetics (octagen, high melting explosive [HMX]; cyclotrimethylenetrinitramine [RDX]; and pentaerythritol tetranitrate [PETN]).

As previously described by Tripathi et al.,[31,32] to obtain valid equilibrium isotherms (following the Langmuir protocol), it is necessary to ensure that a sufficient number of molecules are present at each concentration studied and to allow enough time to reach 99% surface coverage for the given substrate. For all the experiments detailed in this section of the report, the following solution volume and immersion times were used: (1) For concentrations of less than 1×10^{-8} M analyte, 1 L of volume with an immersion time of at least 500 h was used. (2) For concentrations of less than 5×10^{-7} M analyte, 0.5 L of volume with an immersion time of at least 200 h was used. (3) For concentrations including and above 5×10^{-7} M analyte, a solution volume of at least 50 mL with an immersion time of at least 24 h was used. During the equilibration process, the solution was continually shaken to ensure a uniform concentration without gradients.

After equilibrium was achieved, the substrate was transferred to a polystyrene Petri dish with 7 mL of solution at the same concentration to maintain equilibrium. The solution was stirred in the Petri dish using a magnetic stirrer. In a 360 × 360 µm region of the substrate, a total of 36 Raman spectra were collected in a 6 × 6 grid pattern. An integration time of 25 s was used and three measurements were co-added at each point. The substrate was then immersed in a solution of the next higher concentration, and the process was repeated. Figure 22 shows the results of this effort. It appears that as the immersion time increased, the three Raman spectral features observed between the 1220 and 1400 cm^{-1} spectral range seem to increase. However, these features were present in all of the six analytes examined in this work. These features were not present in 4-ATP functionalized Klarite substrate before the addition of analyte aqueous solution. We repeated these experiments, but the results were the same. It was later determined that the Nanopure water (Thermo Fisher Scientific; Waltham, MA) used for this work had some type of impurity and that this impurity was detected. There is a need to revisit this effort with a cleaner water supply.

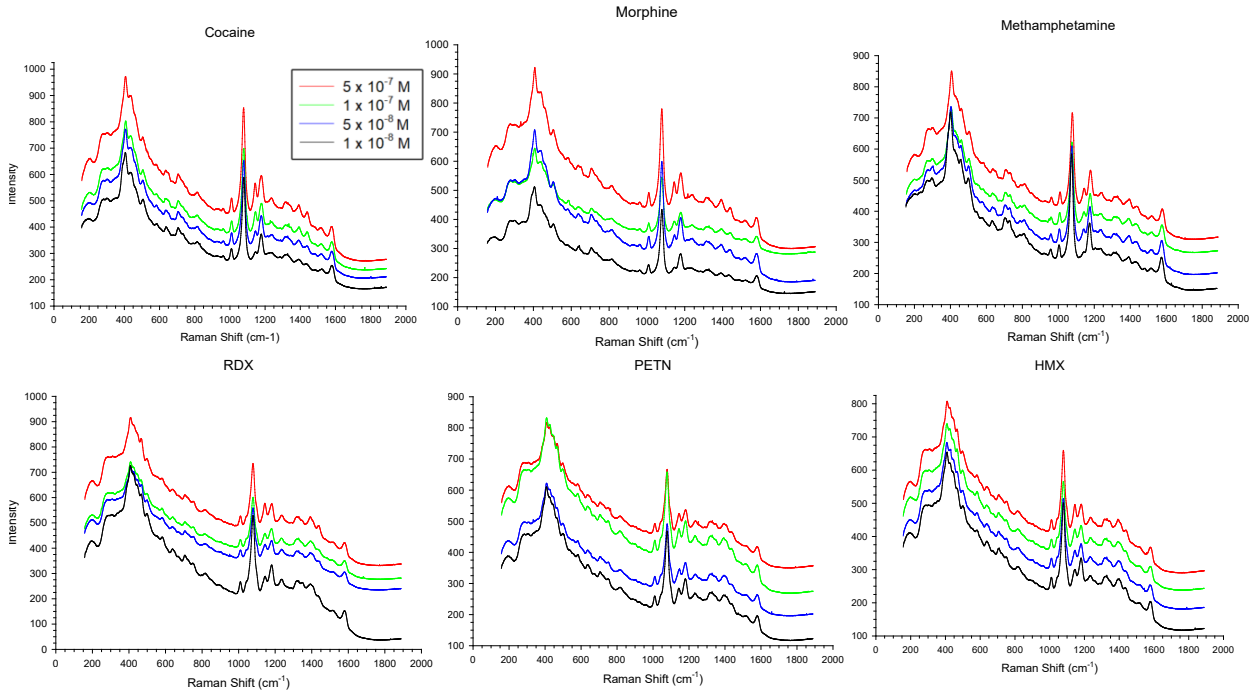

Figure 22. Attempted detection of narcotics and energetics compounds of interest with 4-ATP functionalized Klarite substrate.

3.2 Functionalizing Gold Nanoparticles

In addition to functionalizing planar substrates, we also investigated functionalizing gold nanoparticles with thiolated aptamers. Aptamers are short ssDNA or single-stranded ribonucleic acid (ssRNA) molecules that can selectively bind to a specific target, which includes our drug targets. We contacted a commercial company, RayBiotech Life (Peachtree Corners, GA), to assist us in aptamer selection and modification and in functionalization of the

nanoparticles. We asked them to find an aptamer that could selectively bind methamphetamine. They were going to use the structure-switching SELEX (systemic evolution of ligands by exponential enrichment) method to accomplish this. Based on the results that RayBiotech personnel obtained, it seems that drug and explosive molecules are not well-suited for aptamer capture because they are relatively small molecules with basic structures that lead to minimal structural changes in the aptamer upon target-binding and cause many nonspecific interactions. These characteristics make it difficult to select specific aptamers for a specific small-molecule target.

4. CONCLUSION

In this work, several areas of concern for microfluidics were identified, and potential solutions were investigated with varying levels of success. Unreliable flows were a consistent issue when the attempt was made to use the microfluidic chips with only a vacuum to pull the liquids through the chip. We tried to mitigate this failure by using paper-based microfluidics and by taking active control of the liquids through syringe pumps. The paper-based microfluidics did not actively control the fluid flows and used capillary forces to carry the fluids in the chip. Inconsistent flows became less of an issue, but large background signatures from the paper chip itself proved to be rather challenging. We also attempted to actively pump the fluids using a microfluidic workstation from LabSmith. Syringe pumps allowed us to control the fluids as they were put through the microfluidic chip. However, we still encountered uneven flows and bubbling with the syringe pumps.

The second issue we attempted to remedy was the more-specific binding of our analytes. We had hoped to accomplish this by functionalizing planar substrates and nanoparticles. The planar substrates were treated with 4-ATP and were then exposed to different analytes. During the experiment, it became clear that our water supply was contaminated, which made our experiments unusable. We also attempted to find an aptamer for the targeted binding of methamphetamine, with the aptamer eventually being used to functionalize gold nanoparticles for SERS detection. Unfortunately, the company we asked to develop the aptamer had difficulty selecting a single aptamer they could sequence and reproduce. The fundamental challenges with aptamer development are the small nature of the drug molecules that we are trying to detect and the lack of structural change of the aptamer upon the drug molecule binding to it, which makes it difficult to select an aptamer.

Although microfluidics does hold promise as a portable detection platform, advances still need to be made for more-reproducible flows and for selective binding of analytes in biologically complex matrices.

LITERATURE CITED

1. United Nations Office on Drugs and Crime. Drug Trafficking and the Financing of Terrorism. https://www.unodc.org/unodc/en/frontpage/ (accessed 8 April 2016).

2. National Institute on Drug Abuse. Nationwide Trends. https://www.drugabuse.gov/publications/drugfacts/nationwide-trends (accessed 11 April 2016).

3. Washington Times. Terrorist Organizations Still Profit from Afghan Drug Trade. http://www.washingtontimes.com/news/2013/sep/20/terrorist-organizations-still-profit-afghan-drug-t/ (accessed 11 April 2016).

4. United Nations Office on Drugs and Crime (UNODC). *World Drug Report 2012*; United Nations Publications, Sales No. E.12.XI.1; United Nations: New York, 2012.

5. Stojanovska, N.; Fu, S.L.; Tahtouh, M.; Kelly, T.; Beavis, A.; Kirkbride, K.P. A Review of Impurity Profiling and Synthetic Route of Manufacture of Methylamphetamine, 3,4-Methylenedioxymethylamphetamine, Amphetamine, Dimethylamphetamine and *p*-Methoxyamphetamine. *Forensic Sci. Int.* **2013,** *224* (1–3), 8–26.

6. Cone, E.J. Saliva Testing for Drugs of Abuse. In *Annals of the New York Academy of Sciences*; John Wiley and Sons: Hoboken, NJ, 1993; Vol. 694, pp 91–127.

7. Welter, J.; Meyer, M.R.; Kavanaugh, P.; Maurer, H.H. Studies on the Metabolism and the Detectability of 4-Methyl-amphetamine and Its Isomers 2-Methyl-amphetamine and 3-Methyl-amphetamine in Rat Urine Using GC-MS and LC-(High-Resolution)-MSn. *Anal. Bioanal. Chem.* **2014,** *406* (7), 1957–1974.

8. Strano-Rossi, S.; Leone, D.; de la Torre, X.; Botrè, F. Analysis of Stimulants in Oral Fluid and Urine by Gas Chromatography–Mass Spectrometry II: Pseudophedrine. *J. Anal. Toxicol.* **2010,** *34* (4), 210–215.

9. Gaillard, Y.P.; Cuquel, A.C.; Boucher, A.; Romeuf, L.; Bevalot, F.; Prevosto, J.M.; Menard, J.M. A Fatality Following Ingestion of the Designer Drug Meta-chlorophenylpiperazine (mCPP) in an Asthmatic—HPLC-MS/MS Detection in Biofluids and Hair. *J. Forens. Sci.* **2013,** *58* (1), 263–269.

10. Tehrani, M.S.; Givianrad, M.H.; Mahoor, N. Surfactant-Assisted Dispersive Liquid–Liquid Microextraction Followed by High-Performance Liquid Chromatography for Determination of Amphetamine and Methamphetamine in Urine Samples. *Anal. Methods* **2012,** *4* (5), 1357–1364.

11. Pujol, M.L.; Cirimele, V.; Tritsch, P.J.; Villain, M.; Kintz, P. Evaluation of the IDS One-Step ELISA Kits for the Detection of Illicit Drugs in Hair. *Forensic Sci. Int.* **2007,** *170* (2–3), 189–192.

12. Gottardo, R.; Fanigliulo, A.; Bortolotti, F.; De Paoli, G.; Pascali, J.P.; Tagliaro, F. Broad-Spectrum Toxicological Analysis of Hair Based on Capillary Zone Electrophoresis-Time-of-Flight Mass Spectrometry. *J. Chromatogr. A* **2007,** *1159* (1–2), 190–197.

13. Khan, J.I.; Kennedy, T.J.; Christian, D.R. *Basic Principles of Forensic Chemistry*; Springer: Totowa, NJ, 2012, pp 79–90.

14. Jeanmaire, D.L.; Van Duyne, R.P. Surface Raman Spectroelectrochemistry: Part I. Heterocyclic, Aromatic, and Aliphatic Amines Adsorbed on Anodized Silver Electrode. *J. Electroanal. Chem.* **1977,** *84* (1), 1–20.

15. Moskovits, M. Surface-Enhanced Spectroscopy. *Rev. Mod. Phys.* **1985,** *57* (3), 783–826.

16. Kneipp, J.; Kneipp, H.; Kneipp, K. Two-Photon Vibrational Spectroscopy for Biosciences Based on Surface-Enhanced Hyper-Raman Scattering. *Proc. Natl. Acad. Sci. U.S.A.* **2006,** *103* (46), 17149–17153.

17. Kneipp, K.; Wang, Y.; Kneipp, H.; Perelman, L.T.; Itzkan, I.; Dasari, R.; Field, M.S. Single Molecule Detection Using Surface-Enhanced Raman Scattering (SERS). *Phys. Rev. Lett.* **1997,** *78* (9), 1667–1670.

18. Squires, T.M.; Quake, S.R. Microfluidics: Fluid Physics at the Nanoliter Scale. *Rev. Mod. Phys.* **2005,** *77* (3), 977–1026.

19. Whitesides, G.M. The Origins and the Future of Microfluidics. *Nature* **2006,** *442* (7101), 368–373.

20. Li, B.W.; Jiang, L.; Wang, Q.; Oin, J.H.; Lin, B.C. Micropumps Actuated Negative Pressure Injection for Microchip Electrophoresis. *Electrophoresis* **2008,** *29* (24), 4906–4913.

21. Piorek, B.D.; Lee, S.J.; Moskovits, M.; Meinhart, C.D. Free-Surface Microfluidics/Surface-Enhanced Raman Spectroscopy for Real-Time Trace Vapor Detection of Explosives. *Anal. Chem.* **2012,** *84* (22), 9700–9705.

22. Pallaoro, A.; Hoonejani, M.R.; Braun, G.B.; Meinhart, C.D.; Moskovits, M. Rapid Identification by Surface-Enhanced Raman Spectroscopy of Cancer Cells at Low Concentrations Flowing in a Microfluidic Channel. *ACS Nano* **2015,** *9* (4), 4328–4336.

23. Piorek, B.D.; Andreou, C.; Moskovits, M.; Meinhart, C.D. Discrete Free-Surface Millifluidics for Rapid Capture and Analysis of Airborne Molecules Using Surface-Enhanced Raman Spectroscopy. *Anal. Chem.* **2014,** *86* (2), 1061–1066.

24. Piorek, B.D.; Lee, S.J.; Santiago, J.G.; Moskovits, M.; Banerjee, S.; Meinhart, C.D. Free-Surface Microfluidic Control of Surface-Enhanced Raman Spectroscopy for the Optimized Detection of Airborne Molecules. *Proc. Natl. Acad. Sci.* **2007,** *104* (48), 18898–18901.

25. Andreou, C.; Hoonejani, M.R.; Barmi, M.R.; Moskovits, M.; Meinhart, C.D. Rapid Detection of Drugs of Abuse in Saliva Using Surface-Enhanced Raman Spectroscopy and Microfluidics. *ACS Nano* **2013,** *7* (8), 7157–7164.

26. Talian, I.; Huebner, J. Separation Followed by Direct SERS Detection of Explosives on a Novel Black Silicon Multifunctional Nanostructured Surface Prepared in a Microfluidic Channel. *J. Raman Spectrosc.* **2013,** *44* (4), 536–539.

27. Meier, T.-A.; Poehler, E.; Kemper, F.; Pabst, O.; Jahnke, H.G.; Beckert, E.; Robitzki, A.; Belder, D. Fast Electrically Assisted Regeneration of On-Chip SERS Substrates. *Lab Chip* **2015,** *15* (14), 2923–2927.

28. Lamberti, A.; Virga, A.; Giorgis, F. Microfluidic Electrochemical Growth of Vertically Aligned TiO_2 Nanotubes for SERS Optofluidic Devices. *RSC Adv.* **2015,** *5* (127), 105484–105488.

29. Bailey, M.R.; Pentecost, A.M.; Selimovic, A.; Martin, R.S.; Schultz, Z.D. Sheath-Flow Microfluidic Approach for Combined Surface-Enhanced Raman Scattering and Electrochemical Detection. *Anal. Chem.* **2015,** *87* (8), 4347–4355.

30. Kline, N.D.; Tripathi, A.; Mirsafavi, R.; Pardoe, I.; Moskovits, M.; Meinhart, C.; Guicheteau, J.A.; Christesen, S.D.; Fountain, A.W., III. Optimization of Surface-Enhanced Raman Spectroscopy Conditions for Implementation into a Microfluidic Device for Drug Detection. *Anal. Chem.* **2016,** *88* (21), 10513–10522.

31. Tripathi, A.; Emmons, E.D.; Fountain, A.W., III; Guicheteau, J.A.; Moskovits, M.; Christesen, S.D. Critical Role of Adsorption Equilibria on the Determination of Surface-Enhanced Raman Enhancement. *ACS Nano* **2015,** *9* (1), 584–593.

32. Tripathi, A.; Emmons, E.D.; Kline, N.D.; Christesen, S.D.; Fountain, A.W., III; Guicheteau, J.A. Molecular Structure and Solvent Factors Influencing SERS on Planar Gold Substrates. *J. Phys. Chem. C* **2018,** *122* (18), 10205–10216.

33. Chen, N.; Ding, P.; Shi, Y.; Jin, T.Y.; Su, Y.Y.; Wang, H.Y.; He, Y. Portable and Reliable Surface-Enhanced Raman Scattering Silicon Chip for Signal-On Detection of Trace Trinitrotoluene Explosive in Real Systems. *Anal. Chem.* **2017,** *89* (9), 5072–5078.

Blank

ACRONYMS AND ABBREVIATIONS

4-ATP	4-aminothiophenol
COI	compound of interest
HMX	octagen, high melting explosive
LOD	limit of detection
PBMFD	paper-based microfluidic device
PDMS	polydimethylsiloxane
PETN	pentaerythritol tetranitrate
PLS	partial least squares
RCI	Raman chemical imaging
RDX	cyclotrimethylenetrinitramine
SELEX	systemic evolution of ligands by exponential enrichment
SERS	surface-enhanced Raman spectroscopy
ssDNA	single-stranded DNA
ssRNA	single-stranded RNA
TNT	trinitrotoluene
UCSB	University of California, Santa Barbara
WITec	Wissenschaftliche Instrumente und Technologie GmbH

DISTRIBUTION LIST

The following individuals and organizations were provided with one Adobe portable document format (pdf) electronic version of this report:

U.S. Combat Capabilities Development
Command Chemical Biological Center
(CCDC CBC)
FCDD-CBR-IS
ATTN: Kline, N.
Tripathi, A.
Emmons, E.
Guicheteau, J.
Fountain III, A.

CCDC CBC
Technical Library
FCDD-CBR-L
ATTN: Foppiano, S.
Stein, J.

Defense Technical Information Center
ATTN: DTIC OA

CCDC CBC
FCDD-CBR-IS
ATTN: Vanderbeek, R

U.S. ARMY COMBAT CAPABILITIES DEVELOPMENT COMMAND
CHEMICAL BIOLOGICAL CENTER